ISSN:1306-3111
e-Journal of New World Sciences Academy
2008, Volume: 3, Number: 2
Article Number: A0065

Ahmet Baylar
Cihan Aydın
Mehmet Ünsal
Fahri Özkan
University of Firat
abaylar@firat.edu.tr
Elazig-Turkiye

NATURAL AND APPLIED SCIENCES
CIVIL ENGINEERING/HYDRAULIC
Received: September 2007
Accepted: February 2008
© 2008 www.newwsa.com

CFD ANALYSIS TO PREDICT OPTIMAL AIR INLET HOLE DIAMETER OF VENTURI TUBE IN TERMS OF AIR INJECTION

ABSTRACT

In present paper, the air injection rates of venturi tubes were analyzed using Computational Fluid Dynamics (CFD) modelling. These analyses were carried out by means of FLUENT 6.2 CFD software that uses finite-volume method. There was a good agreement between the measured air injection rates and the values computed from FLUENT 6.2 CFD software. Therefore, the CFD method can be used to estimate optimal air inlet hole diameter of venturi tube that maximizes air injection.

Keywords: CFD, Venturi, Air Injection

VENTURİ TÜPÜNÜN HAVA ENJEKSİYONU AÇISINDAN OPTİMUM HAVA GİRİŞ ÇAPININ CFD ANALİZİ İLE TAHMİNİ

ÖZET

Bu çalışmada, venturi tüplerinin hava enjeksiyon oranları Hesaplamalı Akışkan Dinamiği (CFD) modellemesi kullanılarak analiz edilmiştir. Bu analizler, sonlu hacim metodunu kullanan FLUENT 6.2 CFD paket programı ile yapılmıştır. Ölçülen ve FLUENT 6.2 CFD paket programı kullanılarak hesaplanan hava enjeksiyon oranları arasında iyi bir uyum vardır. Böylece CFD metodu, venturi tüplerin hava enjeksiyonunu maksimize eden optimum hava giriş delik çapını tahmin etmekte kullanılabilir.

Anahtar Kelimeler: CFD, Venturi, Hava Enjeksiyonu

1. INTRODUCTION (GİRİŞ)

Many industrial and environmental processes involve the aeration of a liquid by the entrainment of air bubbles. Venturi aeration is a method of aeration that has become popular in recent years. Recently, Baylar and Emiroglu (2003), Emiroglu and Baylar (2003), Baylar et al. (2005), Bagatur (2005), Ozkan et al. (2006), Baylar and Ozkan (2006) and Baylar et al. (2007a, b) have studied the use of venturi tubes in water aeration systems.

When a minimal amount of differential pressure exists between the inlet and outlet sides of a venturi tube, a vacuum (air suction) occurs at suction holes of venturi tube (Figure 1). When a pressurized operating (motive) fluid, such as water, enters the venturi tube inlet, it constricts toward the throat portion of the venturi tube and changes into a high velocity jet stream. The increase in velocity through the throat portion of the venturi tube, as a result of the differential pressure, results in a decrease in pressure in the throat portion. This pressure drop enables air to be injected through the suction holes and is dynamically entrained into the motive stream. As the jet stream is diffused toward the venturi tube outlet, velocity is reduced and reconverted into pressure energy (but at a level lower than venturi tube inlet pressure). Venturi tubes are high efficient, requiring less than 20% differential to initiate suction.

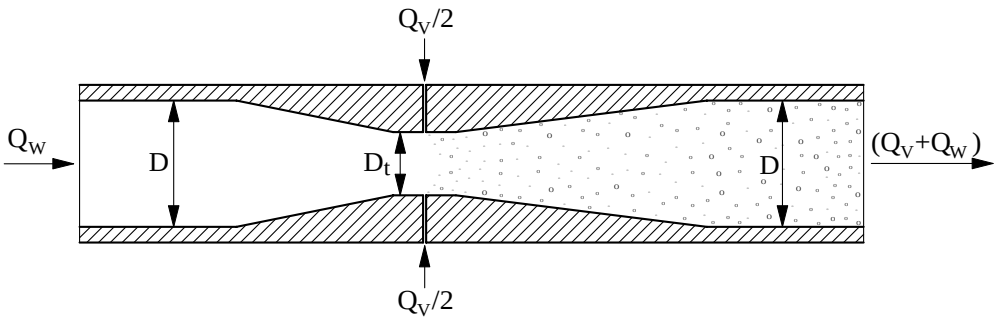

Figure 1. Air suction produced by venturi tube
(Şekil 1. Venturi tüpü ile oluşturulan hava emme)

There are many advantages of using venturi tubes in the water aeration systems. A venturi tube does not require external power to operate. It does not have any moving parts, which increases its life and decreases probability of failure. The venturi tube is usually constructed of plastic and it is resistant to most chemicals. It requires minimal operator attention and maintenance. Since the device is very simple, its cost is low as compared to other equipment of similar function and capability. It is easy to adapt to most of new or existing systems providing that there is sufficient pressure in the system to create the required pressure differential. Because the venturi tube utilizes a vacuum principle rather than a pressure principle, the material being handled is never under high pressure in a concentrated form. This reduces the possibility of caustic chemicals being sprayed into the air through cracks or breaks in the pipe.

In this study, air injection of venturi tube was analyzed using Computational Fluid Dynamics (CFD) modelling. CFD is a well established technique for numerical simulation by which any flow behaviour can be described. The advantage of high-speed and large-memory computers has enabled CFD to obtain solution for many flow problems including compressible or incompressible, laminar or turbulent, reacting or non-reacting, single phase or multiphase, and steady or transient flows.

2. RESEARCH SIGNIFICANCE (ÇALIŞMANIN ÖNEMI)

It is important to predict air injection in venturi tubes because they are used in most water treatment applications for re-oxygenation. This research will investigate whether Computational Fluid Dynamics (CFD) modelling can be used to predict air injection in venturi tubes.

3. VENTURI PRINCIPLE (VENTURİ PRENSİBİ)

The converging tube is an effective device for converting pressure head to velocity head, while the diverging tube converts velocity head to pressure head. The two may be combined to form a venturi tube, named after Venturi, an Italian, who investigated its principle about 1791. It was applied to the measurement of water by Clemens Herschel in 1886. As shown in Figure 2, it consists of a tube with a constricted throat which produces an increased velocity accompanied by a reduction in pressure, followed by a gradually diverging portion in which the velocity is transformed back into pressure with slight friction loss (Daugherty, 1985).

The venturi effect happens due to pressure drop in the throat portion as velocity in the throat portion increases. The increase in velocity V_2 through the throat portion of the venturi tube, as a result of the differential pressure, results in a decrease in pressure p_2 in the throat portion. When the pressure p_2 in the throat portion drops under atmospheric pressure ($p_2<p_{atm}$), air is injected through suction holes and is dynamically entrained into the motive stream.

Writing the Bernoulli equation between section 1 and 2 of Figure 2, we have, for the ideal case,

$$\frac{p_2}{\gamma} = \frac{p_1}{\gamma} + \frac{V_2^2(\beta^2 - 1)}{2g} \qquad (1)$$

where 1 and 2 are subscripts indicating points 1 and 2; p_1 and p_2 are pressures; γ is specific weight; V is velocity at inlet and outlet portion of venturi tube; V_2 is velocity; β is ratio of throat flow area of venturi tube to inlet flow area of venturi tube and g is gravitational acceleration.

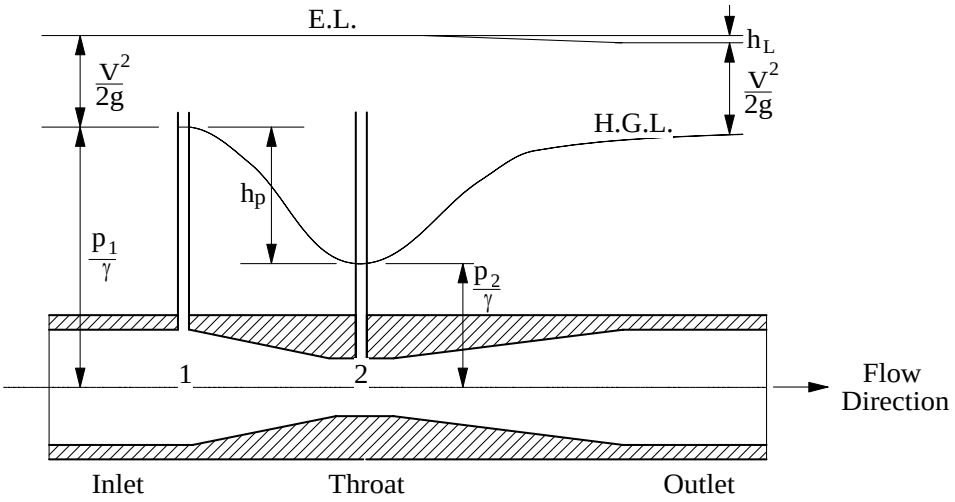

Figure 2. Definition sketch for venturi tube (Daugherty, 1985)
(Şekil 2. Venturi tüpünün tanımı)

4. EXPERIMENTAL DESCRIPTION (DENEYSEL TANIMLAMA)

In this study, the data used were taken from Baylar et al.'s (2007a) experimental study. General view of the experimental setup is

given in Figure 3. For Computational Fluid Dynamics modelling, the venturi tube with inlet and outlet diameters of 42 mm was selected. The ratio of throat diameter of the venturi tube to inlet diameter of the venturi tube, D_t/D, was 0.75. Throat length of the venturi tube was 31.5 mm. The converging cone angle θ_1 and the diverging cone angle θ_2 of the venturi tube were 21° and 7°, respectively. The converging cone angle of 21° and the diverging cone angle of 7° are those that, according to the ASME MFC-3M-1989 (1995), minimize the head losses for a venturi tube. At the throat portion of the venturi tube, two air holes were drilled through the wall. The diameters of these air holes were taken as 3 mm, 6 mm and 12 mm. The Reynolds number was varied between 52000 and 364000.

An air hood for which the plan-view dimensions were 0.70 m x 0.75 m, was used to obtain air entering air holes on venturi tube using an air flowmeter installed on its surface, as illustrated in Figure 3.

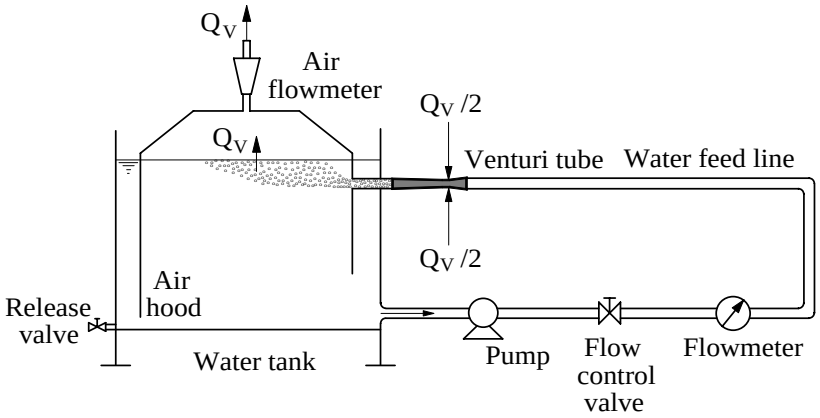

Figure 3. Schematic representation of venturi tube experimental apparatus
(Şekil 3. Venturi tüpü deneysel sisteminin şematik gösterimi)

5. VERIFICATION OF THE CFD STUDY (CFD ÇALIŞMASININ DOĞRULANMASI)

The first step in the uncertainty is numerical verification, which involves determination of numerical errors due to, for example discretisation, iterative and grid nonconvergence, geometry approximations etc. The verification procedure is based on the Freitas (1993), which provides a framework for computational fluid dynamics uncertainty analysis. In this study, the numerical method is formally second-order accurate in space for nodes in the interior of computational grid as reported by Freitas (1993), because the computational efficiency of higher order methods is much greater.

6. ITERATIVE CONVERGENCE (TEKRARLAMALI YAKINSAMA)

Before any discretisation error estimation is calculated, it must be ensured that iterative convergence (if iterative methods are used) is achieved with at least three orders of magnitude decrease in normalized residuals for each equation solved. In this study, the iterative convergence at every time step was checked, and a sample convergence trend is illustrated in Figures 4 and 5.

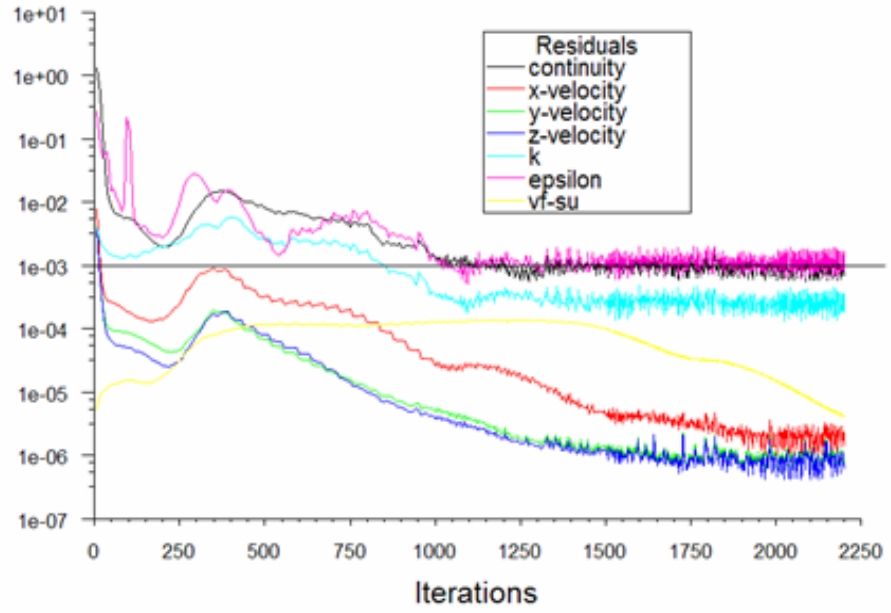

Figure 4. Iterative convergence for Re=156x10^3
(Şekil 4. Re=156x10^3 için tekrarlamalı yakınsama)

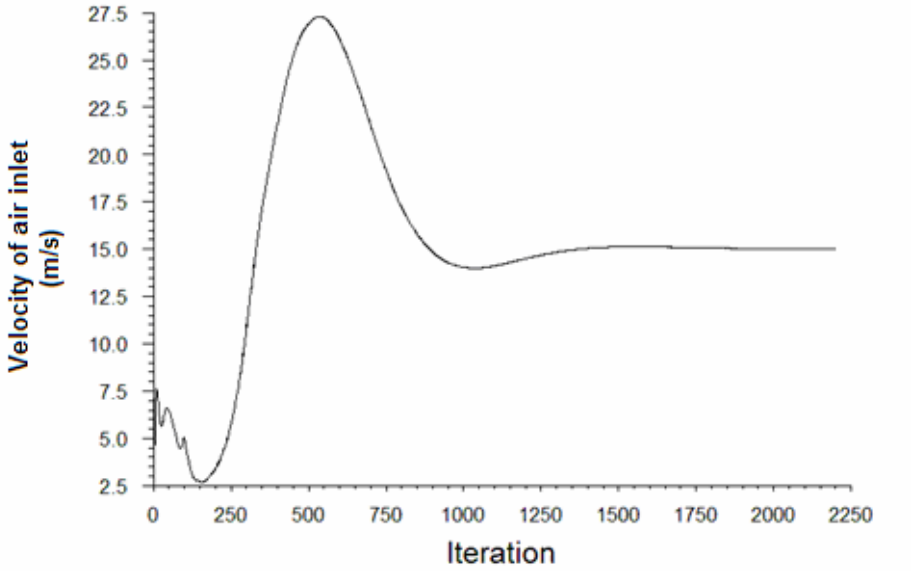

Figure 5. Convergence history of velocity magnitude in air inlet hole for Re=156x10^3
(Şekil 5. Re=156x10^3 için hava giriş deliğindeki hız şiddetinin yakınsaması)

7. GRID CONVERGENCE (GRİD YAKINSAMASI)

The GCI (Grid Convergence Index) method used herein is acceptable and recommended method that has been evaluated over several hundred CFD cases. The GCI was originally proposed by Roache (1994) as a general method for reporting the sensitivity of model solutions to numerical discretisation. It is an index of the uncertainty associated with the solution at particular grid resolution, based on comparison with the solution at another resolution using the theory of generalized Richardson extrapolation (Richardson and Gaunt, 1927). Estimation of grid convergence and the associated uncertainty require a minimum of three grids (Huang et al., 2001).

Three significantly different set of grids are selected and, simulations are run to determine the values of key variables important to the objective of simulation study, for example variable *f* critical to conclusions being reported that herein is the air injection rate. Roache (1994) recommended a minimum %10 change in the grid refined ratio, $r=h_{coarse}/h_{fine}$. Using of geometrically similar cells is preferable. With three grids, labelled from 1=finest to 3=coarsest, $\varepsilon_{32}=f_3-f_2$, $\varepsilon_{21}=f_2-f_1$, $r_{32}=h_3/h_2$ and $r_{21}=h_2/h_1$, the order of accuracy, p of the numerical model can be estimated either iteratively or directly as the following expression if $r_{21} = r_{32} = r$.

$$p = \frac{\left|ln\left|\varepsilon_{32}/\varepsilon_{21}\right|\right|}{ln(r)} \tag{2}$$

In this study, equation (2) was used to estimate the order of accuracy, since r is 1.3 of constant. The approximate relative error can be calculated as following:

$$e_a^{21} = \left|\frac{f_1 - f_2}{f_1}\right| \tag{3}$$

The fine grid convergence index with a safety factor defined by Roache (1994):

$$GCI_{fine} = \frac{1.25 e_a^{21}}{r^p - 1} \tag{4}$$

In Table 2, the discretisation errors is calculated for three selected grids with total number of cells 133230, 84780 and 52444 as 3D tetrahedral and pyramidal elements. Hence, according Table 2, the maximum discretisation uncertainty is 10%, which corresponds to ± 0.76x10^{-3} m^3/s approximately.

Table 2. The calculations of discretisation errors for *d*=6 mm
(Tablo 2. d=6 mm için ayrıklaşma hatalarının hesaplanması)

Re	Q_V x 10^{-3} m^3/s								GCI_{fine}	GCI_{coarse}
x 10^3	f_1	f_2	f_3	ε_{21}	ε_{32}	p	e_a^{21}	e_a^{32}	(%)	(%)
51.95	0.283	0.263	0.253	0.020	0.010	2.53	0.070	0.039	9.3	5.1
103.90	0.571	0.532	0.514	0.039	0.018	3.05	0.068	0.033	7.0	3.4
155.86	0.870	0.828	0.809	0.042	0.019	3.13	0.049	0.023	4.8	2.2
207.81	1.200	1.124	1.096	0.076	0.028	3.86	0.064	0.025	4.5	1.8
259.76	1.633	1.567	1.522	0.066	0.045	1.45	0.040	0.029	10.9	7.8
311.71	1.756	1.673	1.619	0.083	0.054	1.66	0.047	0.032	10.8	7.3
363.67	1.781	1.678	1.622	0.103	0.055	2.38	0.058	0.033	8.4	4.8

8. EFFECT OF TURBULENCE MODEL (TÜRBÜLANS MODELİNİN ETKİSİ)

The four different turbulence model which are standard k-epsilon (2 equations), standard k-omega, RNG k-epsilon and Reynolds stress models (RSM: 7 equations) are used to determine sensitivity of results to turbulence model. According to Figure 6, it is seen that the results from CFD analysis do not considerable change with different turbulence models, and the standard k-epsilon and RSM model are more reliable than other turbulence models. The results with standard k-epsilon and RSM are very close, but RSM takes more CPU time on a per-iteration because of 7 equations. For this reason, in the further CFD analyses, the standard k-epsilon will be preferred as turbulence model in this study.

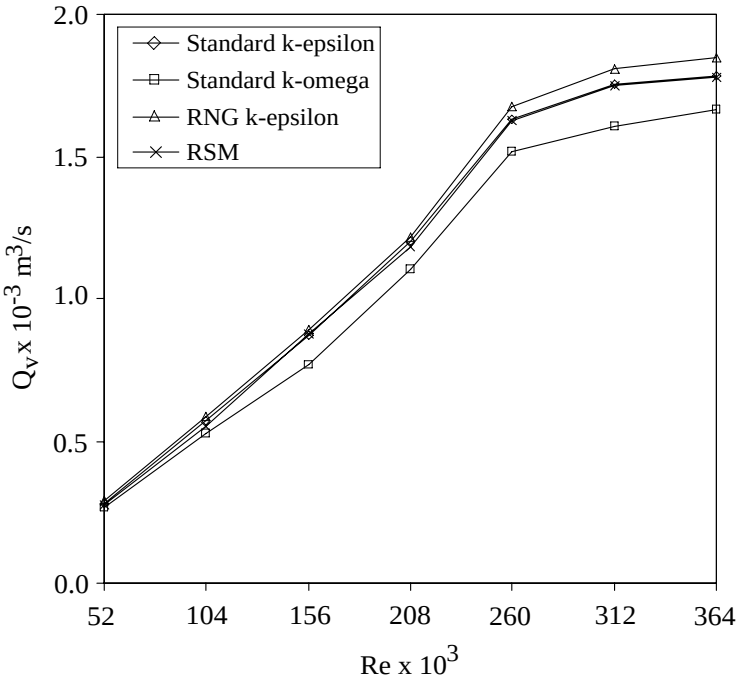

Figure 6. Results derived from different turbulence models
(Şekil 6. Farklı türbülans modellerinden çıkarılan sonuçlar)

9. CFD MODELING OF AIR INJECTION IN VENTURI TUBES (VENTURİ TÜPLERDE HAVA ENJEKSİYONUNUN CFD MODELLEMESİ)

In this study, using Computational Fluid Dynamics (CFD) modelling, the air injection rates of venturi tubes were analyzed. These analyses were carried out by means of FLUENT 6.2 CFD software. FLUENT 6.2 is a Computational Fluid Dynamics software package to simulate fluid flow problems. It uses the finite-volume method to solve the governing equations for a fluid. It provides the capability to use different physical models such as incompressible or compressible, inviscid or viscous, laminar or turbulent, etc.

GAMBIT software is used to do geometry and mesh generation. GAMBIT's single interface for geometry creation and meshing brings together most of FLUENT's preprocessing technologies in one environment (GAMBIT, 2005). In this study, the numerical model geometries were prepared with GAMBIT software and were divided into, approximately, 110,000 3D tetrahedral and pyramidal elements (Figure 7). The size of each cell was defined between 0.5 and 5mm.

In the numerical solutions, 3D multiphase model (Algebraic Slip Mixture Model) and standard k-ε turbulence model were used. The standard k-ε model is a semi-empirical model based on model transport equations for the turbulence kinetic energy (k) and its dissipation rate (ε) (Launder and Spalding, 1972). The model transport equation for k is derived from the exact equation, while the model transport equation for ε was obtained using physical reasoning and bears little resemblance to its mathematically exact counterpart.

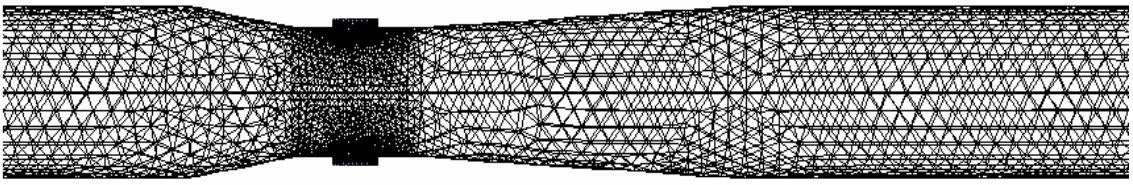

Figure 7. Geometry meshed and detail of venturi tube for D=42 mm; D_t=31.5 mm; d=12 mm
(Şekil 7. D=42 mm; D_t=31.5 mm; d=12 mm'lik venturi tüpü için geometrik ağlar ve detayları)

The algebraic slip mixture model was used in the numerical solutions with FLUENT 6.2 CFD software. The algebraic slip mixture model does not assume that there is an interface between two immiscible phases; it allows the phases to be interpenetrating. Moreover, the algebraic slip mixture model allows the two phases to move at different velocities. The algebraic slip mixture model can solve the continuity equation and the momentum equation for the mixture (FLUENT, 2005).

The continuity equation for the mixture is

$$\frac{\partial}{\partial t}(\rho_m)+\frac{\partial}{\partial x_i}(\rho_m u_{m,i})=0 \tag{5}$$

where ρ_m is mixture density and $\vec{u}_m$ is mass-averaged velocity. No mass transfer is allowed in the algebraic slip mixture model.

The momentum equation for the mixture can be obtained by summing the individual momentum equations for both phases. It can be expressed as

$$\frac{\partial}{\partial t}\rho_m u_{m,j}+\frac{\partial}{\partial x_i}\rho_m u_{m,i}u_{m,j}= \tag{6}$$

$$-\frac{\partial p}{\partial x_j}+\frac{\partial}{\partial x_i}\mu_m\left(\frac{\partial u_{m,i}}{\partial x_j}+\frac{\partial u_{m,j}}{\partial x_i}\right)+\rho_m g_j+F_j+\frac{\partial}{\partial x_i}\sum_{k=1}^{n}\alpha_k\rho_k u_{Dk,i}u_{Dk,j}$$

where n is number of phases; μ_m is viscosity of mixture; F is a body force; α_k is volume fraction of phase k and $\vec{u}_{Dk}$ are drift velocities.

In this study, the velocity inlet boundary condition was applied to determine the water flow rate at the entry of venturi tube. The pressure inlet and the pressure outlet were applied to the boundary of air inlet nozzle and the boundary of outflow of venturi, respectively. The pressure values in the boundary of pressure inlet and outlet were chosen as zero Pascal, so the relative atmospheric pressure was considered in the CFD analyses.

In velocity inlet of boundary,

$$U_n=U_w \tag{7}$$

where, U_n is velocity normal to boundary (m/s) and U_w is mean water velocity (m/s).

Therefore, the water discharge of the venturi tube is defined as:

$$Q_w=U_n A \tag{8}$$

where, A is cross section area of venturi tube with diameter of D.

In this study, the turbulence intensity, I, and the hydraulic diameter were defined as turbulence parameters in the boundary

conditions for k-ε turbulence model. The turbulence intensity, I, is defined as the ratio of the root-mean-square of the velocity fluctuations, to the mean flow velocity. A turbulence intensity of 1% or less is generally considered low and turbulence intensities greater than 10% are considered high. The turbulence intensity at the core of a fully-developed duct flow can be estimated from the following formula derived from an empirical correlation for pipe flows (FLUENT, 2005)

$$I = 0.16\left(Re\right)^{-1/8} \tag{9}$$

At a Reynolds number of 50,000, for example, the turbulence intensity will be 4%, according to equation 9. In this study, generally, the turbulence intensity was estimated between 3%-4%, since the range of Reynolds numbers is 52000-364000. The relationship between the turbulent kinetic energy, k, and turbulence intensity, I, is

$$k = \frac{3}{2}(U_{avg} I)^2 \tag{10}$$

where, U_{avg} is mean flow velocity. If it is known the turbulence length scale, l, turbulence dissipation rate, ε, can be determined from the relationship

$$\varepsilon = C_{\mu}^{3/4} \frac{k^{3/2}}{l} \tag{11}$$

where C_{μ} is an empirical constant specified in turbulence model (approximately 0.09). The turbulence length scale, l, is a physical quantity related to the size of the large eddies that contain the energy in turbulent flows. In fully-developed duct flows, l is restricted by the size of the duct, since the turbulent eddies cannot be larger than the duct. An approximate relationship between the turbulence length scale l and the physical size of the duct is

$$l = 0.07L \tag{12}$$

where L is the diameter of the pipe.

10. CFD MODELLING RESULTS (CFD MODELLEME SONUÇLARI)

The variations in air injection rate Q_V of the venturi tubes with Reynolds number are shown in Fig. 8. Q_V increases with increasing Reynolds number. The primary reason of this is the increased pressure differential between inlet and outlet sides of the venturi tubes as Reynolds number increases (Baylar et al., 2007a).

It is seen from the results that the variation in air inlet hole diameter has a significant effect on Q_V. The values of Q_V increase with increasing air inlet hole diameter up to a certain point and then the values of Q_V remain constant with a further increase of air inlet hole diameter. Thus, the results reveal that air inlet hole diameter of venturi tube plays a significant role in Q_V and there is an optimal air inlet hole diameter of venturi tube that maximizes air injection (Baylar et al., 2007a).

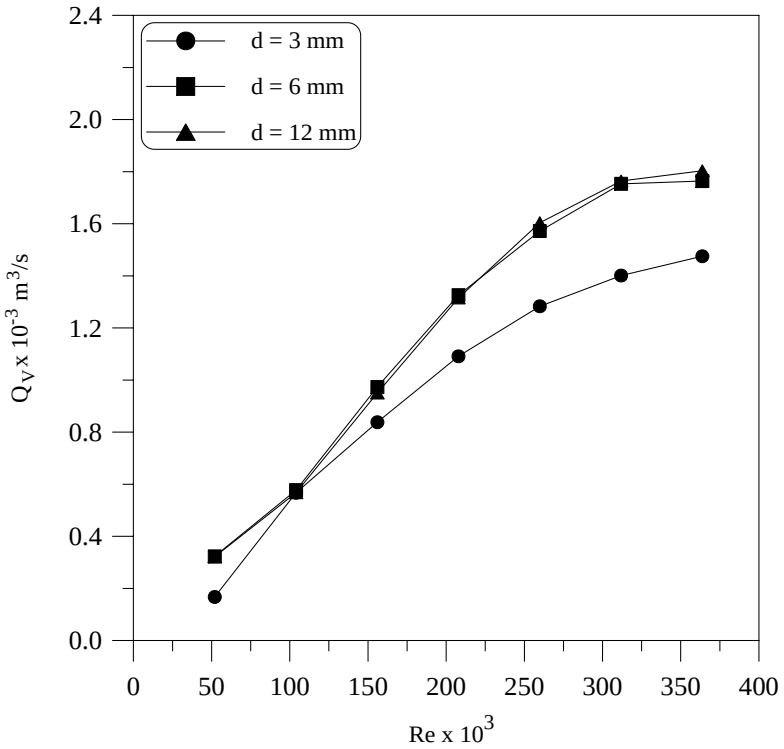

Figure 8. Plot of air injection rate versus Reynolds number for experimental results
(Şekil 8. Deneysel sonuçlar için Reynolds sayısı ile hava enjeksiyon oranının değişimi)

For air inlet hole diameters of 3 mm and 12 mm, static pressure distribution of section and contours of volume fraction of air are showed in Figures 9-10. Moreover, the values computed from FLUENT 6.2 CFD software were compared with Baylar et al.'s (2007a) experimental results, as shown in Figures 11-13. The experimental results and those obtained with FLUENT 6.2 CFD software had generally good agreement with each other. However, for air inlet hole diameter of 12 mm, the values of air injection rate Q_V were less well predicted at high Reynolds numbers. But, the differences between the experimental results and those predicted with FLUENT 6.2 CFD software are at an acceptable level for many uses.

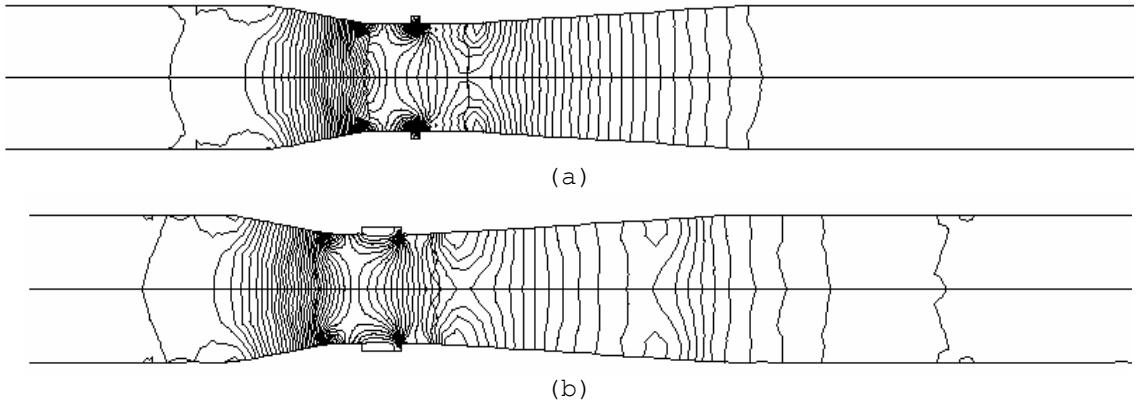

(a)

(b)

Figure 9. Static pressure distribution of section for D=42 mm; D_t=31.5 mm; Q_W=12.11 L/s: (a) d=3 mm; (b) d= 12 mm
(Şekil 9. D=42 mm; D_t=31.5 mm; Q_W=12.11 L/s için statik basınç dağılım bölgeleri: (a) d=3 mm; (b) d= 12 mm)

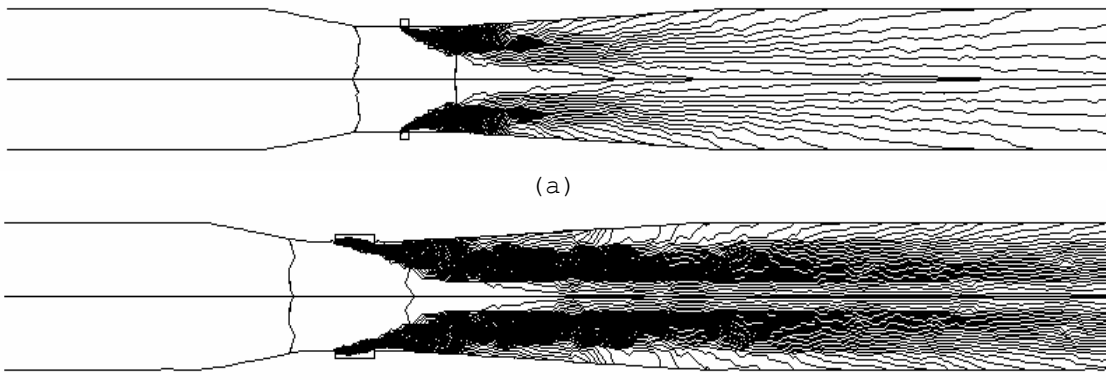

(a)

(b)

Figure 10. Contours of volume fraction of air for D=42 mm; D_t=31.5 mm; Q_W=12.11 L/s:
(a) d=3 mm; (b) d= 12 mm
(Şekil 10. D=42 mm; D_t=31.5 mm; Q_W=12.11 L/s için havanın hacminin konturları: (a) d=3 mm; (b) d= 12 mm)

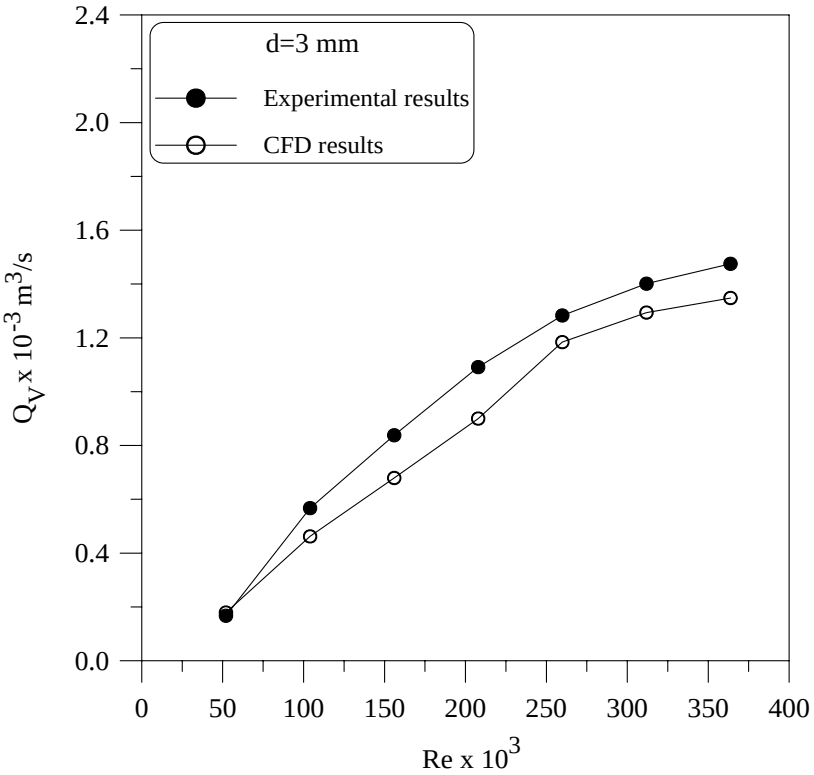

Figure 11. Plot of air injection rate versus Reynolds number for experimental and CFD results (d=3 mm)
(Şekil 11. Deneysel ve CFD sonuçları için Reynolds sayısı ile hava enjeksiyon oranının değişimi (d=3 mm))

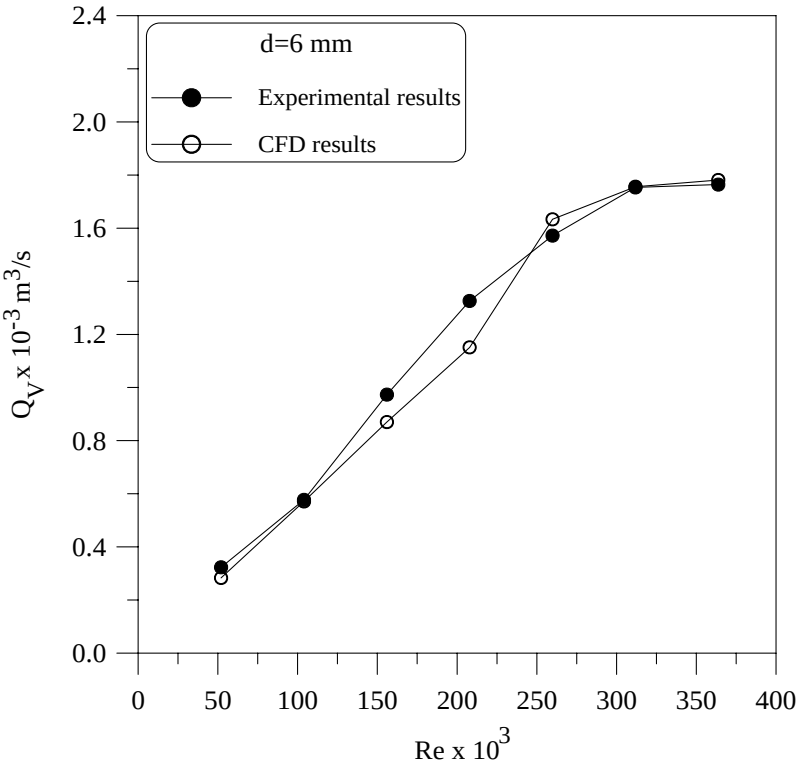

Figure 12. Plot of air injection rate versus Reynolds number for experimental and CFD results (*d*=6 mm)
(Şekil 12. Deneysel ve CFD sonuçları için Reynolds sayısı ile hava enjeksiyon oranının değişimi (*d*=6 mm))

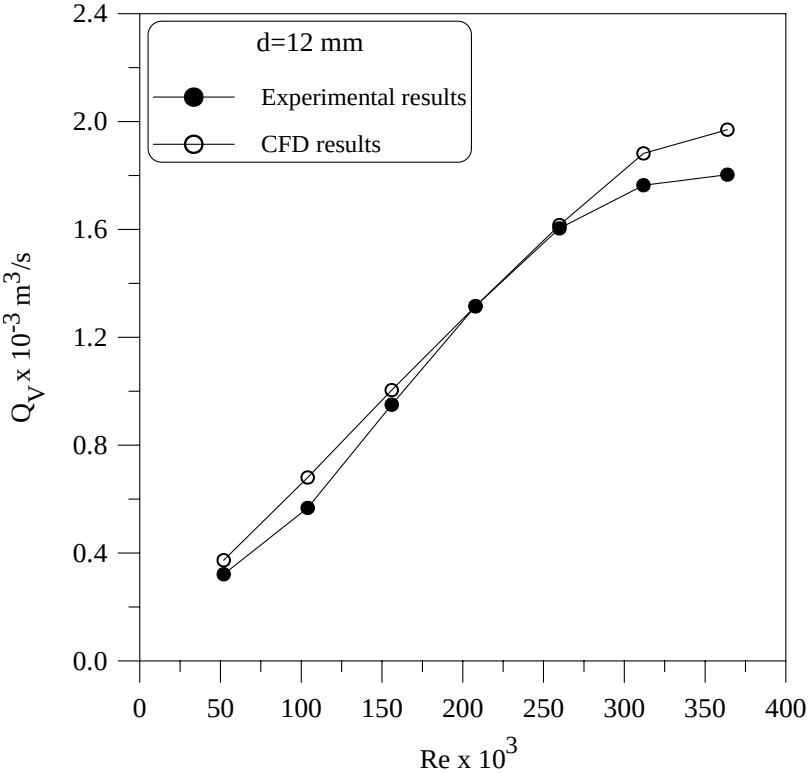

Figure 13. Plot of air injection rate versus Reynolds number for experimental and CFD results (*d*=12 mm)
(Şekil 13. Deneysel ve CFD sonuçları için Reynolds sayısı ile hava enjeksiyon oranının değişimi (*d*=12 mm))

11. CONCLUSIONS (SONUÇLAR)

Investigation of fluid-flow processes can be obtained by two main methods: the experimental investigation and Computational Fluid Dynamics (CFD) modelling. CFD is the discipline in which computers are used to numerically model all flows of interest. In this study, air injection rates of venturi tubes with different air inlet hole diameters were analyzed using CFD modelling. These analyses were carried out by means of FLUENT 6.2 CFD software that uses finite-volume method. There was a good agreement between the measured air injection rates and the values computed from FLUENT 6.2 CFD software. Therefore, the use of the CFD modelling would enable a more practical determination of optimal air inlet hole diameter of venturi tube that maximizes air injection.

REFERENCES (KAYNAKLAR)

- ASME standard MFC-3M-1989. Measurement of fluid flow in pipes using orifice, nozzle and venturi. ASME, Reaffirmed 1995.
- Bagatur, T., (2005). Minimal conditions for venturi aeration of water flows. Proc. Instn Civ. Engrs Water Management, 158 (WM3), pp:127-130.
- Baylar, A. and Emiroglu, M.E., (2003). Air entrainment and oxygen transfer in a venturi. Proc. Instn Civ. Engrs Water and Marit. Engrg. 156 (WM3), pp:249-255.
- Baylar, A. and Ozkan, F., (2006). Applications of venturi principle to water aeration systems. Environmental Fluid Mechanics, 6 (4), pp:341-357.
- Baylar, A., Ozkan, F. and Ozturk, M., (2005). Influence of venturi cone angles on jet aeration systems. Proc. Instn Civ. Engrs Water Management, 158 (WM1), pp:9-16.
- Baylar, A., Ozkan, F. and Unsal, M., (2007a). On the use of venturi tubes in aeration. CLEAN-Soil, Air, Water, 35 (2), pp:183-185.
- Baylar, A., Unsal, M. and Ozkan, F., (2007b). Determination of the optimal location of the air hole in venturi aerators. CLEAN-Soil, Air, Water, 35 (3), pp:246-249.
- Daugherty, R.L., Franzini, J.B. and Finnemore, E.J., (1985). Fluid mechanics with engineering applications. McGraw-Hill, Inc., New York, pp:418-421.
- Emiroglu, M.E. and Baylar, A., (2003). Study of the influence of air holes along length of convergent-divergent passage of a venturi device on aeration. J. Hydr. Res., 41 (5), pp:513-520.
- FLUENT 6.2., (2005). User's guide. FLUENT Inc., Lebanon, NH,
- Freitas, C.J., (1993). Journal of fluids engineering editorial policy statement on the control of numerical accuracy. Journal of Fluids Engineering-Transactions of the ASME, 115 (3), pp:339-340.
- Gambit 2.2., (2005). Modelling guide. FLUENT Inc., Lebanon, NH.
- Huang, J., Lai, Y.G. and Patel, V.C., (2001). Verification and validation of a 3-D numerical model for open-channel flows. Numerical Heat Transfer:Part B:Fundamentals, 40 (5), pp.431-449.
- Launder, B.E. and Spalding, D.B., (1972). Lectures in mathematical models of turbulence. Academic Press, London, England.
- Ozkan, F., Ozturk, M., and Baylar, A., (2006). Experimental investigations of air and liquid injection by venturi tubes. Water and Environment Journal, 20 (3), pp:114-122.

- Richardson, L.F. and Gaunt, J.A., (1927). The deferred approach to the limit. Transactions of the Royal Society of London, 226 (Series A), pp:299-361.
- Roache, P.J., (1994). Perspective-a method for uniform reporting of grid refinement studies. Journal of Fluids Engineering-Transactions of the ASME, 116 (3), pp:405-413.

NOTATION (SİMGE)

A	Flow area of venturi tube
C_μ	Empirical constant specified in turbulence model
d	Air hole diameter
D	Inlet and outlet diameter of venturi tube
D_t	Diameter of venturi tube at throat portion
e_a	Relative error
F	Body force
f	Considered variable
g	Gravitational acceleration
GCI	Grid convergence index
h	Mesh size
h_p	Difference of pressures p_1-p_2
I	Turbulence intensity
k	Turbulence kinetic energy
l	Turbulence length scale
L	Relevant dimension of duct
n	Number of phases
p	Order of accuracy
p_1	Pressure at inlet portion of venturi tube
p_2	Pressure at throat portion of venturi tube
p_{atm}	Atmospheric pressure
Q_v	Volumetric flow rate of air entering air holes on venturi tube
Q_w	Water flow discharge
r	Grid refinement ratio
Re	Reynolds number at inlet portion of venturi tube
$\vec{u}_{Dk}$	Drift velocities
$\vec{u}_m$	Mass-averaged velocity
U_{avg}	Mean flow velocity
U_n	Velocity normal to boundary
U_w	Mean water velocity
V	Velocity at inlet and outlet portion of venturi tube
V_2	Velocity at throat portion of venturi tube
β	Ratio of throat flow area of venturi tube to inlet flow area of venturi tube
γ	Specific weight
θ_1	Converging cone angle of venturi tube
θ_2	Diverging cone angle of venturi tube
α_k	Volume fraction of phase k
ε	Turbulence dissipation rate
ε_{ij}	Grid convergence error between solutions of two grids
μ_m	Viscosity of mixture
ρ_m	Mixture density